



Since January 2020 Elsevier has created a COVID-19 resource centre with free information in English and Mandarin on the novel coronavirus COVID-19. The COVID-19 resource centre is hosted on Elsevier Connect, the company's public news and information website.

Elsevier hereby grants permission to make all its COVID-19-related research that is available on the COVID-19 resource centre - including this research content - immediately available in PubMed Central and other publicly funded repositories, such as the WHO COVID database with rights for unrestricted research re-use and analyses in any form or by any means with acknowledgement of the original source. These permissions are granted for free by Elsevier for as long as the COVID-19 resource centre remains active.



Numerical evaluation on indoor environment quality during high numbers of occupied passengers in the departure hall of an airport terminal

Yu Zhao, Yao Feng, Liangdong Ma^{*}

School of Civil Engineering, Faculty of Infrastructure Engineering, Dalian University of Technology, 2 Linggong Road, Ganjingzi District, Dalian, 116024, China

ARTICLE INFO

Keywords:

Airport terminal
Airflow organization
Thermal environment
Predicted mean vote
Aerosol

ABSTRACT

The rapid development of airports and the rapid spread of coronavirus disease 2019 (COVID-19) have brought increased attention to indoor environment quality, airflow organization, key pollutant dispersion, and ventilation modes in airport terminals. However, the characteristics of these parameters, especially carbon dioxide (CO₂) and aerosol diffusion, are not fully understood. Therefore, in this study, the airflow patterns; CO₂ and aerosol dispersion; and several thermal environment indices, including temperature, wind velocity, and predicted mean vote (PMV), of an airport terminal departure hall with high numbers of occupied passenger were numerically evaluated using the realizable $k-\epsilon$ and passive scalar models. The efficacies of three common ventilation modes, namely, up-supply and up-return, up-supply and down-return with different sides, and up-supply and down-return with the same side, were evaluated based on the CO₂ removal efficiency and spreading range of aerosols. The results indicated that under high numbers of occupied passenger conditions, these ventilation modes vary slightly, with respect to create a comfortable and healthy environment. In particular, the up-supply and down-return with different sides mode was the best among the modes considered, when comparing the indices of temperature, wind speed PMV, and CO₂ emission efficiency. Conversely, with respect to decreasing the risk of aerosol exposure, the up-supply and down-return with the same side mode was the best. Overall, the results from this study provide fundamental information for predicting CO₂ and aerosol exposure levels and will act as a reference for the design and operation of ventilation systems in airport terminal buildings.

1. Introduction

Since the 1990s, China's airports have rapidly developed, and the construction volume of major regional airport terminals has doubled in the past 10 years [1]. Many airport terminals throughout China are currently undergoing or are facing reconstruction and expansion, including the Guangzhou Baiyun Airport, Xi'an Xianyang Airport, and Shanghai Pudong Airport [2]. In addition, the People's Daily reported that China will build more than 30 new airports in the next three years [2]. Further, the rapid development of civil aviation airport terminals in China has made airplanes an indispensable means of transportation. Statistics show that the average annual passenger throughput of the top 10 hub airports in Asia ranges from 42,902,520 to 97,794,207 passengers [3], indicating that

^{*} Corresponding author.

E-mail address: liangdma@dlut.edu.cn (L. Ma).

people use airport terminals more frequently in today's climate. Thus, large numbers of passengers waiting for flights in airport terminals are quite common in metropolitan areas, including Beijing, Shanghai, and Guangzhou. However, because airport terminals generally are large spaces, sometimes the ventilation form and air distribution design inside terminals are not effective enough in supplying fresh air and exhausting pollutants.

The outbreak of coronavirus disease 2019 (COVID-19) highlighted the importance of ventilation in buildings. Previously, to a smaller extent, the severe acute respiratory syndrome virus in 2003, the Middle East respiratory syndrome virus in 2012, and other respiratory infectious diseases forced airport operators to pay attention to the problem of indoor air quality. Since 2021, local epidemics have occurred in Shijiazhuang, Shenzhen, Nanjing, Haikou, and Shanghai, and the "breakthroughs" are all related to international airports. The international airport has become an important place for the spread of the epidemic [4]. It is generally believed that droplets or aerosols produced by people's breathing or other activities are carriers for virus transmission [5], and people are infected by inhaling droplets or aerosols with viral DNA or RNA. In general, infected people transmit virus particles during breathing, speaking, coughing, or sneezing [5–7]. As an important public place, airports are characterized by high occupancy flows. The high personnel density, long stay time, poor ventilation effect and long exposure time result in a greater exposure risk of pollutants, compared to other environments. Meanwhile, due to the characteristics of high numbers of occupied passenger, once an epidemic breaks out at the airport, it will cause the rapid expansion and large-scale spread, which will consume a lot of manpower, material and financial resources to eliminate it, causing great economic losses and social impact. Just as the failure of prevention and control of the epidemic at Nanjing Lukou Airport in 2021, causing the epidemic to spread to 5 provinces and 9 cities [8]. Therefore, the higher the risk of pollution transmission inside the airport and the serious consequences of the epidemic once it occurs, the related research is crucial. The environment construction in the airport terminals must incorporate the requirements of both human thermal comfort and good health with low transmission of infectious diseases.

In the past 20 years, many scholars have conducted extensive research regarding ventilation form, air distribution, and air quality inside airport terminals. Regarding the indoor environment of an airport terminal, numerous studies have measured and investigated the thermal environment and human thermal comfort level in different areas by employing indices associated with the temperature, wind speed, thermal comfort predicted mean vote (PMV) and Predicted Percent Dissatisfied (PPD) [9–13]. According to field measurements from nearly 30 airport terminals in China, one survey found that the air-conditioning load of a terminal building has a significant correlation with the air-conditioning system. Field surveys of eight airports revealed that even if the forms of the cooling and air conditioning systems are the same, a difference in their arrangement has a notable effect on the airflow organization [1]. Extensive field surveys in three airport terminal buildings in the United Kingdom demonstrated the effect of the thermal environment on overall comfort and revealed consistent discrepancies [14]. Thus, a reasonable displacement of the ventilation systems could be beneficial for building a comfortable thermal environment in airport terminals. In conclusion, current researches are mostly based on thermal environmental parameters such as temperature and wind speed, and less attention has been paid to other pollutants such as CO₂ and aerosols. However, as the world is increasingly concerned about environmental and health safety issues, it is not enough to only consider thermal environmental parameters. Research on the pollutants when evaluating the effectiveness of ventilation systems is necessary and urgent, especially at the airport terminals with high numbers of occupied passenger.

Environmental health is also an important consideration when evaluating the environmental quality of airport terminals. Among various types of pollutants, the key pollutants affecting air quality and human respiration in the environment are carbon dioxide (CO₂) and particulate matter (PM). Regarding aerosols or particles produced by human respiration, many studies have shown that particle size ranges from 0.01 μm to 2000 μm [5–7,15–21]. During speaking, coughing, and sneezing processes, larger size particles may be produced, whereas during breathing processes, particles sized 0.01 μm–5 μm are mainly produced.

Other scholars have studied the effects of various pollutants, including CO₂ and PM, in airport environments. Over the past three decades, CO₂ has continuously been considered to be an important indicator in the evaluation of the air sanitation status of airports. Wang et al. showed that the air quality satisfaction of passengers is highly correlated with the CO₂ concentration of an airport terminal [22]. Using the post assessment method, an indoor environmental quality test of 11 terminals in eight airports covering five climatic regions in China revealed that the indoor environmental quality of typical airport terminals in China basically meet current regulation standards [23], in which the indoor thermal environment compliance rate was higher than 70% and the average volume fraction of CO₂ was no more than 700 ppm [24]. Based on long-term CO₂ concentration monitoring data, Hong et al. proposed that the median values of CO₂ concentration were lower than 550 ppm, except for the remote departure lounge. They believed that passive ventilation also plays an important role in diluting pollutants [25]. While evaluating the air infiltration efficacy of a hub airport terminal building, Liu et al. found that for the CO₂ concentration, no obvious stratification characteristics were observed on different floors. Their results showed that the average values were 507 ppm, 532 ppm, and 648 ppm in the winter, spring, and summer, respectively [26]. Note that the concentration of CO₂ in the terminal building in the summer was significantly higher than that in other seasons. In another study, it was found that the CO₂ concentration in an airport terminal was 480–965 ppm, wherein the highest concentrations were observed at night, particularly at midnight. According to the airport's flight plans, flight traffic and passenger flow are the most intense during these hours [27]. The study also showed that the more crowded the terminal, the higher the CO₂ concentration. However, this level did not exceed 1000 ppm, indicating that the ventilation system worked effectively [27]. Ren conducted long-term online monitoring of indoor and outdoor PM_{2.5} and ultra-fine particle (UFP) concentrations in Tianjin airport terminals. Studies have shown that the seasonal variation of indoor PM_{2.5} concentrations is significant; however, the concentration of UFPs remains relatively stable in different seasons [28]. According to an air quality test of 9 large hub airports in the United States, the average PM_{2.5} levels of airports with designated smoking areas and smoke-free airports are 11.5 μg/m³ (range: 2.2–29.0 μg/m³) and 8.0 μg/m³ (range: 2–15.2 μg/m³), respectively [29]. The particle number concentrations in airport terminals present a bimodal size distribution that is completely different from the size distribution measured in a normal urban environment. Specifically, the total UFP exposure of passengers during

their entire waiting period is approximately equivalent to the exposure of 11 h in a normal urban environment [30,31]. Kim et al. [32] and Zanni et al. [33] monitored the PM contents and passenger flow inside and outside of airports and found that passenger traffic has an impact on airborne contaminants in terminal buildings.

Overall, various studies have evaluated airport ventilation systems and airflow organization using thermal comfort as an indicator. However, research focusing on CO₂, aerosol, and PM concentrations in airport terminals, especially under high occupancy conditions, is limited. Further, the pollutant dispersion and discharge efficiency of ventilation systems under situations with high numbers of occupied passenger are not yet fully understood.

Therefore, the purpose of this study was to evaluate the airflow organization of a ventilation system based on the distributions of temperature, wind speed, PMV, and key pollutants (including CO₂ and aerosols) at high numbers of occupied passenger airport terminals. To date, three main approaches have been employed to monitor thermal environment factors and pollutant patterns in airport environments: (1) field measurements, (2) particle image velocimetry (PIV) measurements, and (3) computational fluid dynamics (CFD) simulations. Considering the disadvantages of time consumption and poor repeatability for field and PIV measurements, the CFD technique is a suitable method with reasonable simulation precision and flexible repeatability. Thus, the CFD algorithm with the realizable $k-\varepsilon$ turbulence closure scheme was adopted in this study. In addition, a Euler-Euler two fluid flow model was employed to simulate the dispersion of CO₂ and aerosols. The significance of this study is the consideration of CO₂ and aerosols when evaluating the efficiency of ventilation systems in airport terminals. The results of this study will provide guidance and act as a basis for the design and operation of ventilation systems in airport terminals and other similarly enclosed spaces with high numbers of occupied passenger.

2. Methodology

2.1. Turbulent flow model

The realizable $k-\varepsilon$ developed by Shih et al. [34] has been proven to perform well for a variety of flow conditions, including vortices, rotations, round jets, and thermal buoyancy plume [35–37], suitable for indoor environment modeling in terms of accuracy, computing efficiency and robustness [38–41]. The accuracy of results in our previous studies [42–46] is also acceptable to truly reflect turbulence and pollutant dispersion patterns. Thus, we also used the realizable $k-\varepsilon$ turbulence model to simulate wind flow in a terminal waiting area. The governing equations include the continuity equation, momentum equation, energy equation, turbulent kinetic equation, and turbulent dissipation rate equation, which are expressed in Eq. (1). Note that based on the Boussinesq approximation, the velocity and temperature fields were coupled.

$$\frac{\partial(\rho\Phi)}{\partial\tau} + \text{div}(\rho\mathbf{U}\Phi) = \text{div}(\Gamma\mathbf{grad}\Phi) + S \quad (1)$$

where ρ is the fluid density (kg/m³); Φ is a general variable that represents the velocity components u (m²/s), v (m²/s), and w (m²/s) in the momentum equation; T (°C) is the temperature in the energy equation; k is the turbulent kinetic energy (J) in the turbulent kinetic equation; ε is the dissipation rate in the turbulent dissipation rate equation, τ is the time (s); div indicates divergence; \mathbf{U} is the velocity vector; Γ is the generalized diffusion coefficient; \mathbf{grad} represents gradient; and S is the generalized source phase.

2.2. Pollutants from breathing and transport models

Owing to the high numbers of occupied passenger in airports, the pollutants produced by the human body are the main contributors and must be considered when studying the ventilation system and pollutant diffusion of airports. CO₂ is an important indicator for evaluating air quality, and droplets and aerosol particles produced by respiration are important carriers of virus transmission. Currently, there are two particle stress analysis methods: models based on discrete particles (particle track or Euler–Lagrangian) or dual-fluid (Euler–Euler) models. The Euler-Euler model is a kinetic model for treating particles as continuous phases, and there are many studies [47–49] on the pollutant simulation by employing the abovementioned model. Some related studies show that the Euler-Euler model is acceptable for the motion prediction of small particles by comparing the numerical simulation results with the experimental results. Therefore, this study adopted the Euler–Euler model to predict contaminants diffusion including aerosol particles, which is proposed by Ref. [50]. In this study, the numerical simulation of particle dispersion was accomplished assuming the following three points.

- The effect of particles on turbulent flow was assumed to be negligible because of the low particle volume fraction in the airflow. Interaction between the air and particles was treated as a one-way coupling, in which the air affected the particles.
- All particles were spherical, and the particle density was constant. According to the study by Ref. [51], the density of particle could be considered 1003 kg/m³.
- Only deposition was included as a source term during particle dispersion modeling.

2.2.1. Pollutant diffusion model

Because it is difficult to simulate particle diffusion and time constraints, the pollutant distribution considers several discrete categories (where the particle size is constant), wherein the particle properties are treated as scalars (e.g., particle concentration). In each discrete particle category, the control transmission equation describing the CO₂ and particle transmission is as follows:

$$\frac{\partial C}{\partial t} + \frac{\partial}{\partial x_i} \left[u_i C - (D + \tau_p) \frac{\partial C}{\partial x_i} \right] = S \quad (2)$$

where C represents the CO₂ or particle concentration, t is the time, x_i ($i = 1, 2, 3$) represents the directions of the three coordinates, u_i is the average air velocity component in three dimensions, D is the molecular diffusivity of the CO₂ or particle, τ_p is the turbulent diffusivity of the CO₂ or particle, and S is the rate of change of the dispersion source phase. For CO₂, S has only diffusion source phase, and for particles, S includes diffusion source and deposition source phase.

The main influencing factors in particle movement are evaporation, deposition, resuspension and coagulation. The droplet evaporation process is mainly affected by two factors, the size of the droplet size and the relative humidity (RH) at the indoor environment. It can be seen that droplets with sizes of less than 5 μm completely evaporate within a few milliseconds, even under the conditions of high RH conditions [52,53]. Meanwhile, the airport ground is relatively clean and our simulation is a seated human body with small perturbations, the resuspension for particles is minimal and can be ignored in our study. In addition, Rim et al. [54] found that coagulation should be considered during high concentration periods ($>20,000 \text{ cm}^{-3}$) by analyzing the effects of coagulation, deposition and ventilation in the indoor environment on the changes in particle attenuation. Since our research is on the distribution characteristics of aerosols in the terminal under steady-state conditions, the particle size is 0.01–2.62 μm and the concentration is not high, the coagulation process could also be ignored. Thus, only the deposition characteristic of particles is considered as a sink source during particle dispersion process.

Molecular diffusivity is a constant of proportionality that relates the flux of gas pollutants to the concentration gradient. This relationship is termed Fick's first law of dispersion. For CO₂, the molecular diffusion coefficient can be determined using the following equation:

$$D = \frac{435.7T^{3/2}}{P(V_A^{1/3} + V_B^{1/3})^2} \sqrt{\frac{1}{\mu_A} + \frac{1}{\mu_B}} \times 10^{-4} \quad (3)$$

where T is the temperature (K); p is the atmospheric pressure (101,325 Pa); V_A and V_B are the molar volumes at the normal boiling point for gases A and B, respectively, and μ_A and μ_B are the molecular weights for gases A and B, respectively.

For nanoscale particles, especially particles less than 100 nm, the Brownian diffusion of particles caused by the random thermal motion of gas molecules is distinct. According to Fick's first law, the particle Brownian diffusivity D is given as:

$$D = \frac{k_B T C_C}{3\pi\mu d_p} \quad (4)$$

where k_B is the Boltzmann constant ($1.3807 \times 10^{-23} \text{ J K}^{-1}$), T is the air temperature (K), C_C is the Cunningham slip correction coefficient of particles, μ is the aerodynamic viscosity (Nm^{-2}), and d_p is the particle diameter (m). The Cunningham slip correction coefficient of the particles can be calculated using the following equation:

$$C_c = 1 + \frac{\lambda}{d_p} \left[2.514 + 0.800 \exp\left(-0.55 \frac{d_p}{\lambda}\right) \right] \quad (5)$$

where λ is the average free path of an air molecule (m). To solve Eq. (5), turbulent flow can be treated as an ideal gas flow as follows:

$$\lambda = \frac{k_B T}{\sqrt{2}\pi d^2 p} \quad (6)$$

where k_B is the Boltzmann's constant ($1.3807 \times 10^{-23} \text{ J K}^{-1}$), T is the ambient temperature (K), d is the air molecular diameter (m), and p is the atmospheric pressure (Pa).

To calculate the turbulent diffusivity τ_p of the pollutants, the turbulent Schmidt number Sc_t , which is defined as the ratio of the turbulent momentum diffusivity ν_t to the turbulent diffusivity τ_p of the pollutants, is used:

$$Sc_t = \frac{\nu_t}{\tau_p} \quad (7)$$

The law of particle turbulent diffusion is very complex, as it is affected by the particle size and turbulence degree of the flow field. Currently, studies mainly use the analogy method with the gas turbulent diffusion coefficient to determine the turbulent diffusion coefficient of particles. In this study, the turbulence dispersion coefficient of the particles was determined by applying the Hinze-Tchen equation to calculate the particle turbulent diffusion coefficient, as shown in Eq. (8):

$$\frac{\nu_p}{\nu_t} = \left(1 + \frac{\tau_p}{\tau_t} \right)^{-1} \quad (8)$$

where ν_p is the particle turbulent dispersion coefficient (m^2s^{-1}), ν_t is the air turbulent dispersion coefficient ($\text{m}^2 \text{s}^{-1}$), and τ_p is the particle relaxation time (s), which is given by:

$$\tau_p = \frac{\rho_p d_p^2 C_c}{18\mu} \quad (9)$$

where ρ_p represents particle density. Furthermore, τ_t is the air turbulence fluctuation time (s), which can be calculated using the

following equation:

$$\tau_t = \sqrt{\frac{3}{2}} C_\mu^{3/4} \frac{k}{\varepsilon} \tag{10}$$

where C_μ is the empirical constant, K is the turbulent kinetic energy, and ε is the turbulent dissipation rate. For the particle size range considered in this study, $\tau_p/\tau_t \leq 1$, $\nu_p = \nu_t$. The value of ν_t was computed by solving the Reynolds-averaged Navier–Stokes (RANS) equations using the proposed k - ε turbulence model.

2.2.2. Particle deposition model

To ensure a comprehensive calculation, the deposition model was applied to the field function, and the source term (S_c) of the deposition-induced particle diffusion was calculated using the field function method, as follows:

$$S_c = -kC_{dp} \tag{11}$$

The weighted average of the particle deposition fluxes in all directions was calculated according to the method proposed by Corner and Pendlebury [55], wherein the weighted average deposition rate of particles settling on each surface of the closed space is determined as follows [56]:

$$k = \frac{V_{dv}A_v + V_{du}A_u + V_{dd}A_d}{V} \tag{12}$$

where k is the weighted average deposition rate of particles (s^{-1}), A_v is the area of the vertical surface (m^2), A_u is the area of the upper surface facing the normal direction (m^2), A_d is the area of the lower surface facing the normal direction (m^2), V is the volume of the enclosed space (m^3). V_{dv} , V_{du} , V_{dd} is the deposition rate of different surfaces, calculated in the supporting information.

3. Model description

3.1. Model geometry

In this study, we established a geometric model using the terminal building of the Dalian Zhoushuizi International Airport as the research object. Owing to the complex internal structure of the terminal building, this model ignores areas in the terminal building that have little effect on the airflow. Because of the large size of the airport terminal building, only part of the west side of the terminal was selected as the simulation object. A simplified terminal model was established, for which the details are as follows. The waiting area we

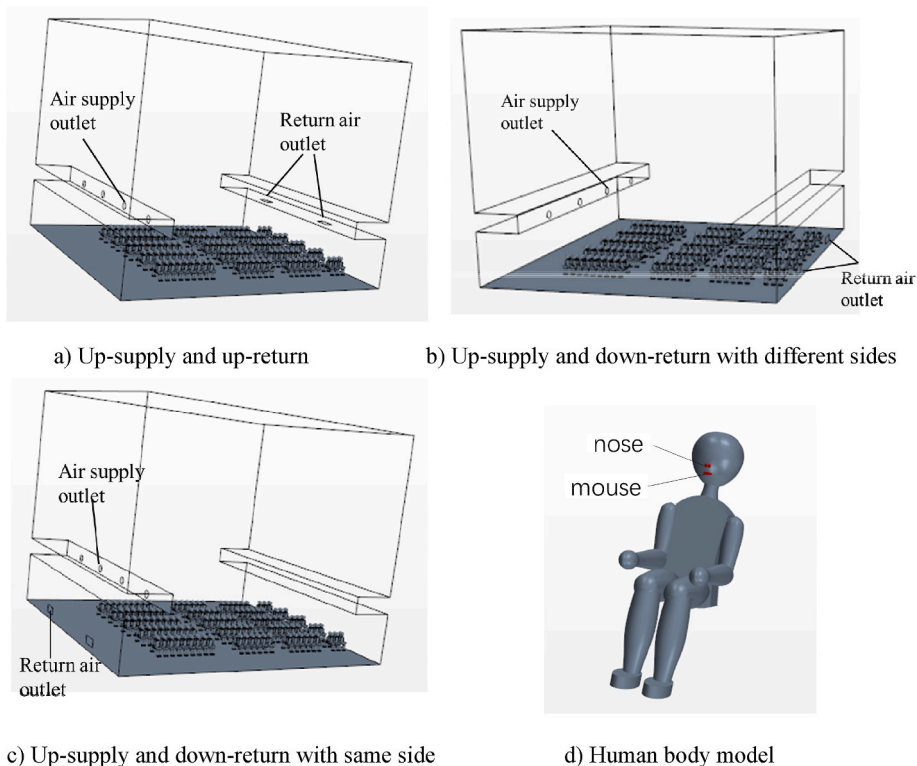


Fig. 1. Geometric and human body models.

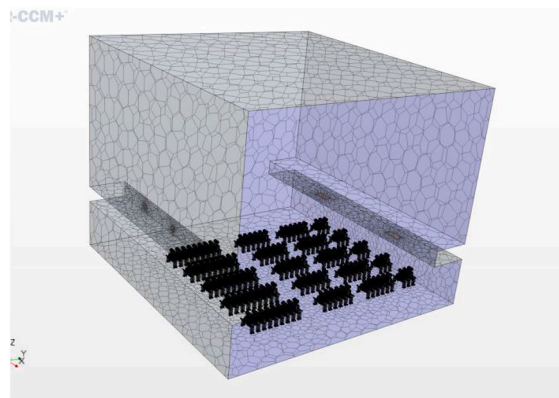
selected was a 25 m × 24 m × 20 m geometric model. The air supply inlet is a circular nozzle with a diameter of 630 mm placed 3.5 m from the wall and 5 m above the ground, while the return air outlets are 1500 mm × 650 mm louver return air vents placed 0.5 m or 4.5 m from the ground.

The airport terminals are usually tall and large spaces, unlike common offices, hotels and other buildings, and diffusers are rarely used for air supply. Through extensive literature reading, the nozzle air supply is the most commonly used method in airport terminals [57–61]. In addition, there is currently a new form of air-conditioning with radiant floor and displacement ventilation system applied to airport terminals. However, other airports are less used except Bangkok International Airport, Hamburg International Airport in Germany and Xi'an Xianyang International Airport [62]. Based on the above mentioned, in our research, we have selected the most commonly used the nozzle air supply, and designed three common air supply methods: (1) up-supply and up-return, wherein there is a supply air outlet at the top and a return air outlet at the top of the opposite wall; (2) up-supply and down-return with different sides, wherein there is a supply air outlet at the top and a return air outlet at the bottom of the opposite wall; and (3) up-supply and down-return with the same side, wherein there is a supply air outlet at the top and a return air outlet at the bottom of the same wall.

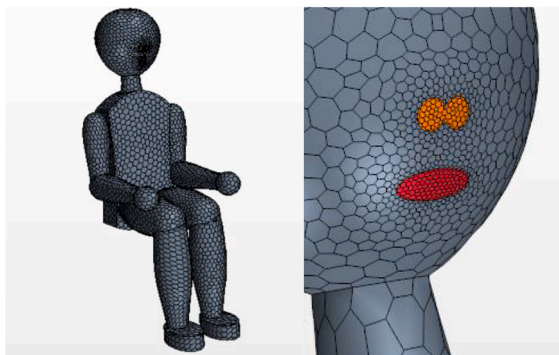
For passengers in the terminal, we established a 1:1:1 geometric model according to the sitting size of adults. The height of the human body is approximately 1.5 m, the length of the head is approximately 0.37 m, the maximum head radius is 0.17 m, and the length of the upper body is approximately 0.7 m. The nose is simplified as two circles with $r = 0.005$ m, and the mouth is simplified as an ellipse with a primary radius of 0.03 m and a secondary radius of 0.02 m. The geometric and human body models are shown in Fig. 1.

3.2. CFD mesh establishment and simulation conditions

After the model was established, it was necessary to mesh the model. The speed, precision, and convergence of the simulation calculations are closely related to the quality of the mesh. In this study, STAR-CCM+ software was used to mesh the model. The mesh model used was an unstructured mesh and was used for the surface reconstruction. The mesh generator included a polyhedral mesh generator and a prism-layer mesh generator. The basic size of the grid was 2 m, and custom grid sizes were set in specific areas, such as the air supply outlet, return air outlet, and surface of the human body, for encryption. For the manikin, the mouth area is approximately $1.884 \times 10^{-3} \text{ m}^2$ with 117 refined surface meshes and the nose area is approximately $5 \times 10^{-5} \text{ m}^2$ with 81 refined surface



a) Grid of the department hall



b) Human mesh and partial enlargement

Fig. 2. Calculation model meshing diagram.

meshes. To overcome the disadvantages of the Realizable $k-\epsilon$ model when simulating low Reynolds number flows within the near-wall region, all y^+ Wall Treatments were also used in the study [63]. The all y^+ wall treatment is a hybrid treatment that attempts to emulate the high-wall treatment for coarse meshes, and the low-wall treatment for fine meshes. It is also formulated with the desirable characteristic of producing reasonable answers for meshes of intermediate resolution (that is, when the wall-cell centroid falls within the buffer region of the boundary layer). According to the simulation results, y^+ value surrounding the human body was in the range of 0.3–1. The grid diagram of the waiting area and human body, as well as the local enlargement diagram, are shown in Fig. 2.

The supply air outlet is defined as the velocity inlet boundary condition, and the return air outlet is defined as the pressure outlet boundary condition. Moreover, the east side wall of the model was set as a flow-slip outlet condition, while the ceiling, floor, and other walls were set to have non-slip and adiabatic wall conditions. For the human body, the mouth was defined as a velocity inlet boundary condition, and the nose was defined as a pressure outlet boundary condition. The detailed calculation parameters are as follows:

- (1) According to the airport design specifications, the indoor design temperature in the summer is 26 °C, and the fresh air ratio is 30%. Therefore, the supply air temperature was set to 18 °C.
- (2) According to the national standards of the People's Republic of China, when the passenger density is less than or equal to 0.4 people/m², the minimum required fresh air volume/person is 19 m³/(h-person) [23]. Thus, the supply air speed was set to 3.39 m/s.
- (3) Human body heat dissipation is related to many factors such as gender, age, clothing, labor intensity, and environmental conditions. According to the literature [64], in a state of extremely light work, like people in an environment such as an office, a hotel or a waiting hall, the human body emits about 134 W of heat, of which radiation, convection, and latent heat account for 40%, 20%, and 20%, respectively. The surface area of the human body is approximately 1.6–2.0 m². Thus, the human body was set to have a constant heat flow boundary of 71.7 W/m².
- (4) A stable situation was considered in our study. In the steady state, we think that talking is a more common behavior than coughing, sneezing, etc. Thus we set a steady exhalation airflow to represent talking. According to the research of [65] on the respiratory rate of Chinese residents, we set the exhalation speed of the human mouth to be 0.58 m/s, and the nose inhales with a constant pressure of -0.217 Pa.
- (5) The CO₂ concentration in the exhaled air of the human body was 3.6% (36,000 ppm) [66].
- (6) The particle size data in Table 1 are obtained from the study of respiratory aerosols and droplets by Ref. [5], and we added the original figure to Fig. S1 in the supporting information. Owing to the complexity and inconvenience during the simulation, the continuous particle size distribution was divided into nine discrete categories. The division rule is based on the distribution characteristics of the particle size, where the particle size range is finer and coarser near the peak and off-peak sections of particle concentration. The nine particle size partitions were then selected as 0–22 nm, 22–28 nm, 28–45 nm, 45–90 nm, 90–225 nm, 225–330 nm, 330–1004 nm, 1004–2042 nm and 2042–3000 nm. The particle size in Table 1 is the median particle size of each partitions.
- (7) As mentioned above in the manuscript, only deposition was considered in the particle dispersion simulation. Thus, for the boundaries including the wall and human body, particles are deposited when touching the boundaries. In addition, when simulating aerosol particle dispersion patterns, only one infected patient located at 6 different positions in Fig. 13 exhaled the viral aerosols using mouth at a constant flow, and that other healthy persons only inhaled the aerosols using nose. Meanwhile, particles at the air supply outlet is set to 0 to represent the air supply is virus-free.

To evaluate the ability and robustness of the established numerical model in simulating CO₂, particle diffusion, and deposition, we conducted independent tests on the grid. For the simulation calculations, we established models with approximately 1.88 million, 3.49 million, and 5.57 million grids, respectively. The initial and boundary conditions of the grid tests were the same as those previously described. The simulation results are shown in Fig. 3. By analyzing the average values at different height planes, the wind speed and CO₂ concentration distributions were found to be quite similar under different grid numbers, among which any obvious differences were less than 10%. This proves that the use of the 3,448,863 polyhedral grids for numerical simulation ensured calculation accuracy and improved simulation efficiency.

In this study, the commercial CFD analysis software STAR-CCM+ was used for the simulation, and the realizable $k-\epsilon$ model was used to simulate parameters such as flow velocity, pressure, and turbulence in the air flow field. A passive scalar model was used to solve for

Table 1
Human breathing conditions.

Particle diameter (nm)	Particle number concentration (10 ⁴ m ⁻³)	Exhalation conditions		Inspiratory conditions	
		Temperature (°C)	Velocity (m/s)	Temperature (°C)	Pressure (Pa)
11	4.81	34	0.58	26	-0.217
25	44.8				
36	201				
67	364				
157	194				
277	75.6				
668	22.3				
1523	2.08				
2618	0.169				

the CO₂ and PM concentrations. To calculate the convection term in the control equation and the pressure-flow coupling format, we used the second-order upwind style and SIMPLE formats, respectively. When the residuals of the continuity equation and the energy equation were $\leq 10^{-6}$, and the residuals of other equations were $\leq 10^{-4}$, the numerical simulation is considered to be convergent. Thus, when the average temperature, speed, pressure, CO₂ concentration, PM concentration, and other parameter values of the entire calculation area are stable, the numerical simulation is convergent.

3.3. Model validation

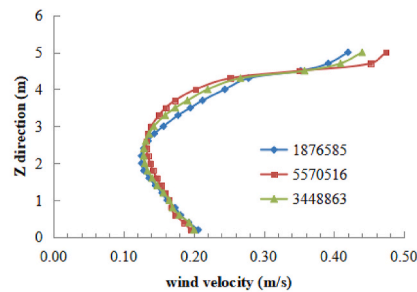
It is important to evaluate the validity of the model by comparing the results of the numerical simulations with real measurements. In our study, the concentrations of CO₂ and PM2.5 in the arrival hall of the Zhoushuizi Airport were measured using existing instruments to verify the model. In addition, we measured some parameters of the air outlet for model verification.

To verify the model, we conducted an actual measurement at the arrival hall of the airport. Briefly, after counting the passenger flow of the airport over a day, we set the monitoring time to 12:00–20:00 every day. Four measuring points were set up in the arrival hall of the airport to monitor the temperature, wind speed, CO₂ concentration, and PM concentration at each location. The floor plan of the airport arrival hall is shown in Fig. 4. Two points 1 and 4 are set near the two arrival exits A and B in the arrival hall. Meanwhile, considering a uniform distribution of the measuring points, the points 2 and 3 are set in the middle area of the arrival hall. The measuring point 2 located in the middle of one seated area, as shown in Fig. 4 b), the measuring point 3 located at an empty area of the hall, not close to any rest area. In addition, considering the height of the breathing area of the passengers, various test instruments were arranged on tripods at a height of 1.2 m. The mobile sampling system are shown in Fig. 4. To determine the changes in passenger flow in the seating area, a camera was placed nearby to take video.

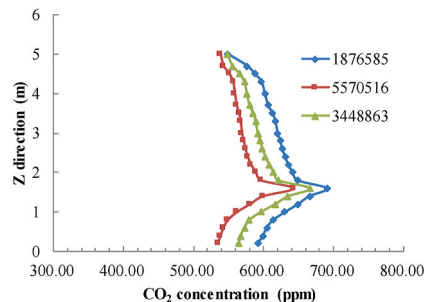
We conducted model verification using a model established in the arrival hall on the first floor of the terminal building. The size of the geometric model was 210 m × 20 m × 3.8 m. Other conditions, such as the air supply outlet and human body model, are described in Section 3.1. In addition, the penetration at the entrance of the terminal building in model verification was considered. During the actual measurement, the permeability coefficient was 0.7942 [67], and the outdoor atmospheric PM2.5 particle concentration was 6.12 μg/m³ calculated by the Air Quality Index in the weather forecast. The geometric model used for model verification is shown in Fig. 5.

The middle seat area in the arrival hall and the time period when the flow of people is stable were used for model verification. The size of the geometric model was 32 m × 20 m × 3.8 m. Other conditions, such as the air supply outlet and human body model, are described in Section 3.1. The geometric model used for model verification is shown in Fig. 5.

The model verification results are listed in Fig. 6. These results are consistent with the field measurement results, and the maximum relative error is less than 10%, which is the general accuracy requirement for model prediction. Therefore, the model has sufficient accuracy for the further analysis of pollutant diffusion in the airport environment.

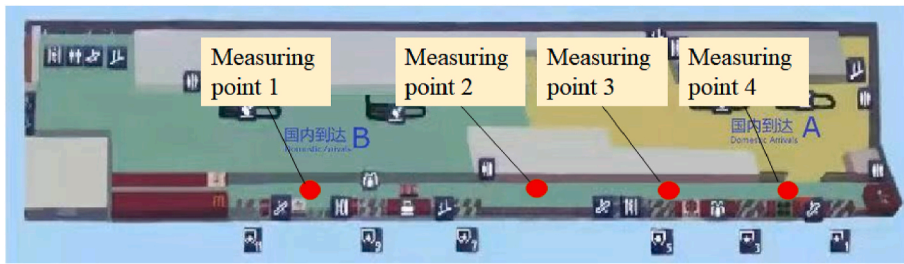


a) Mesh independence test (average velocity at different height planes)



b) Mesh independence test (average CO₂ concentrations at different height plane)

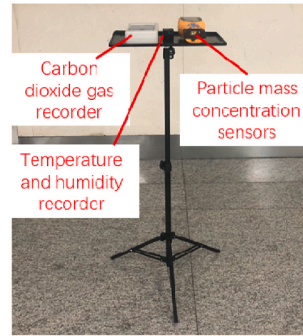
Fig. 3. Mesh independence tests.



a) Floor plan of airport arrival hall



b) Real picture of the measuring point 2 position



c) Mobile sampling system

Fig. 4. Schematic of field measurement area and actual sampling system.

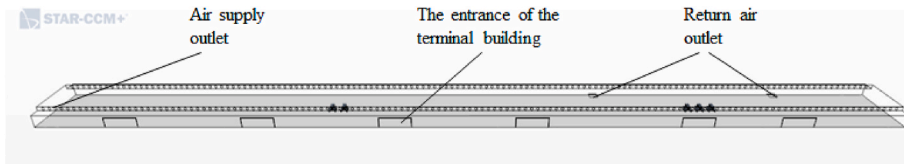


Fig. 5. Geometric model used for model verification.

4. Results and discussion

In the following sections, we consider two regions for analysis. One region is the “Department hall”, referring to the entire area. The other region is the “Respiratory region” considering the sitting state, referring to the area of 1–1.5 m in the vertical direction.

To facilitate the analysis, we also establish three auxiliary planes in the simulation. One cross-section is the height of the 1.2 m horizontal surface considering the respiratory height of the occupied passengers, one section is a vertical surface cut off from near the top return air outlet, and one section is the vertical surface of the display streamline cut out from the center of the return air outlet. The associated charts are shown in the Supporting Information, Fig. S2.

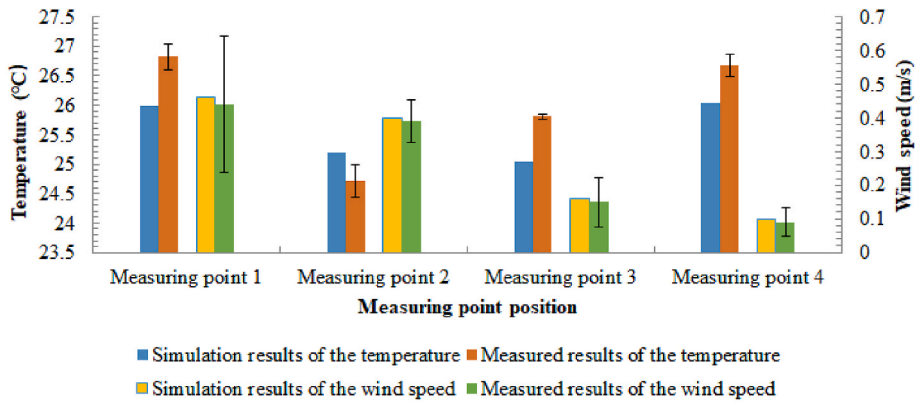
4.1. Temperature patterns

4.1.1. Temperature analysis at the respiratory range

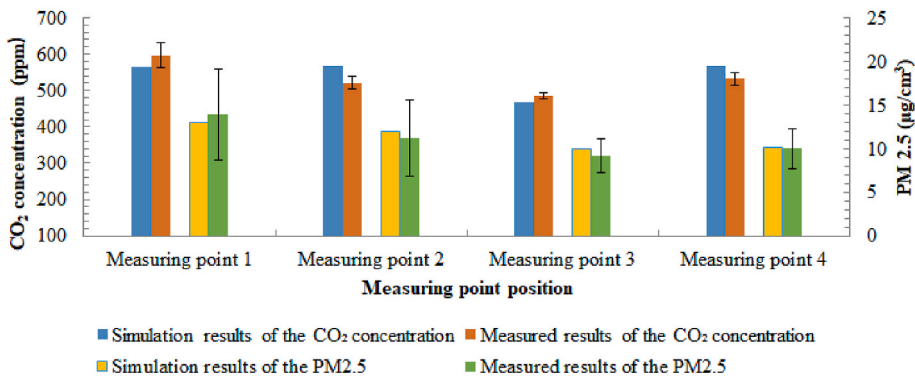
As there are rest seats in the department hall for passengers waiting for their plane, a height of 1.2 m was considered to be the plane of human breathing. Fig. 7 shows the temperature field distribution characteristics of the 1.2 m height plane under the three ventilation modes considered. Overall, the temperature in most regions of the breathing plane was maintained at 25–28 °C, which is similar to Huang et al.’s simulation results of Guangzhou Baiyun Airport [68]. Moreover, the temperatures in some areas close to the human body were obviously higher because temperature of the air exhaled by the human body is 34 °C, which increases the temperature of the airport terminal. In each of the three ventilation modes, the temperature on the side close to the air outlet was generally higher, which may indicate that the air outlet was too high, causing airflow to only weakly affect the area below the air outlet. As Zhao et al. once proposed, the position of the air outlet at the airport should be lowered a bit [62].

4.1.2. Temperature analysis across the entire department hall

To clarify the thermal plume near the human body, the temperature distribution at vertical plane with the height no more than 4 m is shown in Fig. 8. The detailed location of the cross-section in the model could be found in Fig. S2 at the Supporting Information. It can



a) Thermal environment parameter in the model validation



b) pollutant concentration in the model validation

Fig. 6. Model validation results.

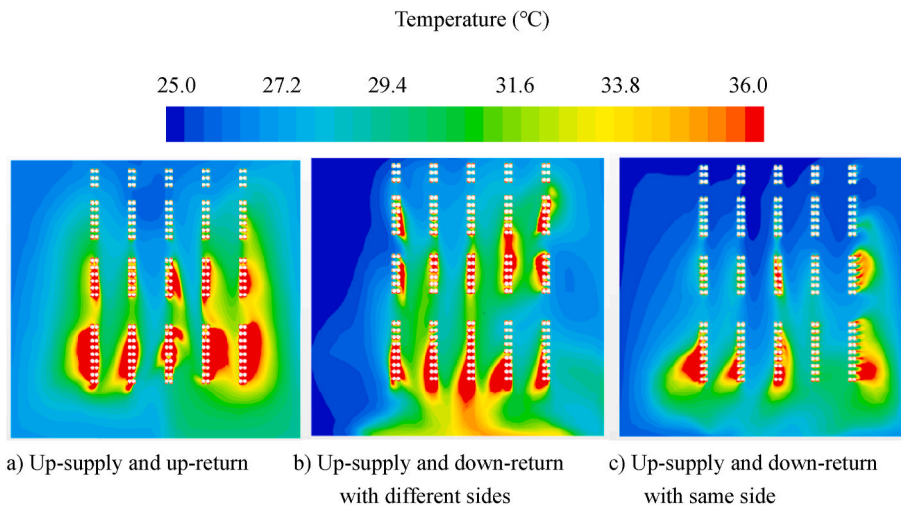


Fig. 7. The 1.2 m height plane temperature field of three ventilation forms.

be seen that in the up-supply and up-return ventilation method and up-supply and down-return with different sides ventilation method, there are significant upward human thermal plume near the human body. That is because the air outlet in the opposite side of the air flow did not sink significantly at the abovementioned two ventilation modes, the thermal plume around the human body

developed without restriction. However, when ventilation is the up-supply and down-return with same side, the upward trend of the thermal plume near the human body is not obvious, more concentrated on the human body surface. That is due to the significant downward airflow in the lower region along ventilation direction at the up-supply and down-return with same side ventilation mode, and the upward thermal plume is not obvious due to the compression of the downward airflow, which could also be found in Fig. 10.

Considering the breathing height of the human body when sitting, the respiratory region vertical height was set within the range of 1–1.5 m for analysis. Table 2 lists the comparison results between the temperature in the department hall and the temperature in the respiratory region.

As listed in Table 2, the temperatures in the respiratory region were 3.3 °C, 2.3 °C, and 1.9 °C higher than those in the department hall, for the up-supply and up-return, up-supply and down-return with different sides, and up-supply and down-return with same side modes, respectively. These higher temperatures may be because of the high density of people under high numbers of occupied passenger, which increases heat dissipation. This indicates that passenger flow is an important factor affecting temperature in airport terminals.

When the ventilation mode was up-supply and down-return on the same side, the temperature in the department hall was the lowest, and the temperature difference between the respiratory region and the department hall was the smallest, indicating that the air-conditioning system plays the best regulatory role in this ventilation mode. When the ventilation mode was up-supply and up-return, the temperature in the respiratory region was almost 30 °C, which is much higher than the summer indoor design temperature of 26 °C. Therefore, this ventilation mode is unfavorable.

4.2. Wind velocity

4.2.1. Wind velocity analysis at the respiratory range

Fig. 9 shows the distribution characteristics of the wind speed field at the 1.5 m height plane under the three ventilation forms. The indoor wind speed of the comfort air-conditioning in the summer should be ≤ 0.3 m/s [23]. The wind speed cloud chart shown in Fig. 9 shows that most areas in the terminal meet this requirement. Specifically, when the ventilation mode was up-supply and down-return with different sides, the wind speed distribution in the breathing plane of the department hall was the most uniform, and the area where the wind speed was greater than 0.2 m/s was less than that of the other two air supply modes. Further, the wind speed distribution characteristics show that the wind speed near the return air outlet is too high, reaching as high as 0.5 m/s.

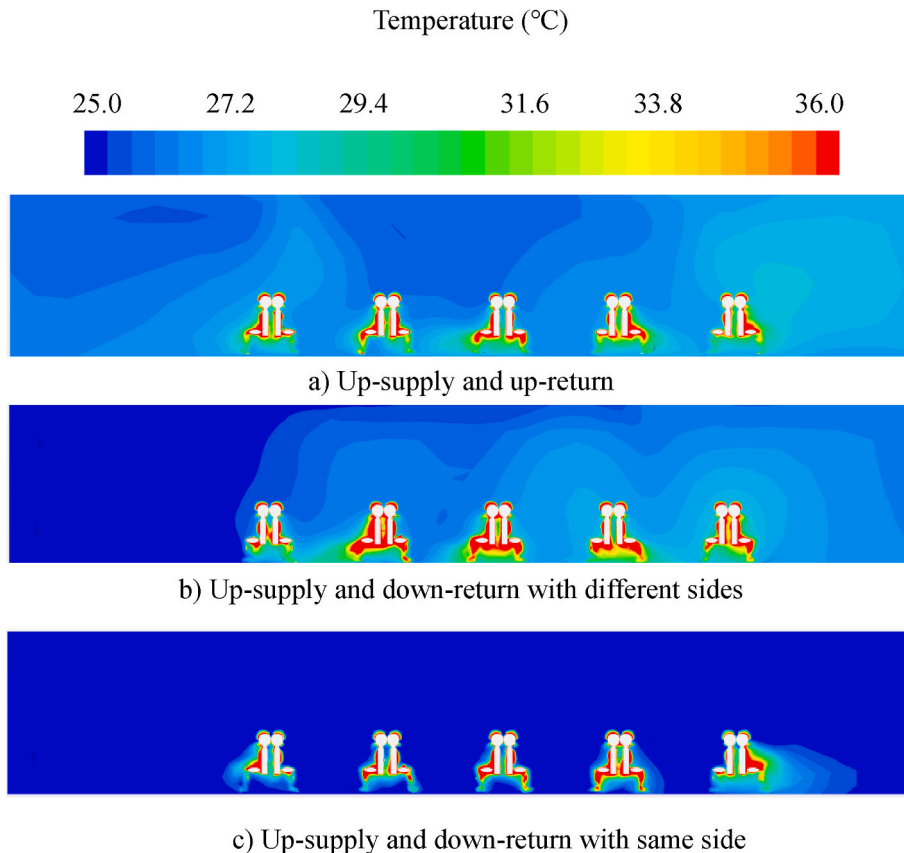


Fig. 8. Temperature distribution of the vertical the vertical direction near the human body.

Table 2
Average temperature of three ventilation forms (°C).

	Up-supply and up-return	Up-supply and down-return with different sides	Up-supply and down-return with same side
Department hall	26.4	26.1	25.2
Respiratory region	29.7	28.4	27.1

4.2.2. Wind velocity analysis of the entire department hall

For clearly identify the difference among three different airflow patterns, a vertical cross-section at the center of one return airflow outlet(The location was shown in Fig. S2 at the supporting information) was established and the airflow vectors were shown in Fig. 10. It could be concluded that a significant stagnant wake appeared at the bottom left of Fig. 10 for the ventilation modes except the up-supply and down-return with same side mode. As the representative 1.2 m horizontal surface just transected the stagnant wake areas, due to low airflow disturbances and poor cooling effect, it seems to be reasonable when obtaining the high temperature, significant thermal plume and high PMV values at the bottom of Figs. 7 and 8 a), 8 b) and 11, respectively. Meanwhile, an obvious downward trend of wind velocity, especially at the areas far away from the supply air outlet, appeared when the ventilation mode is up-supply and down-return with same side. Those strong downward flow could significantly suppress the thermal plume around human bodies, which is consistent with the temperature distribution in Fig. 8 c). In addition, although the ventilation rate among three ventilation modes is the same, the differences in airflow patterns also deeply influenced the pollutant dispersion and aerosol transmission.

The average wind speeds of the three ventilation modes in the department hall and the respiratory region are shown in Table 3. For these modes, the wind speed in the department hall was between 0.12 m/s and 0.18 m/s, and the wind speed in the breathing zone was between 0.10 m/s and 0.16 m/s. The wind speed in the breathing zone under each ventilation mode was approximately 0.02 lower than that in the entire department hall. The large number of passengers may cause the wind speed in the respiratory region to decrease. By comparing the average wind speeds of the three types of ventilation, it is obvious that the slowest wind speed is that of up-supply and down-return with different sides mode, followed by the up-supply mode and up-return and the up-supply and down-return with the same side mode. The results show that up-supply and down-return with different sides is the best form of ventilation, as it does not impose a strong sense of blowing.

4.3. PMV analysis

PMV is a comprehensive evaluation index based on the basic equation of human thermal balance and the grade of psychophysiological subjective thermal sensation. PMV index has been numerously verified to be correct when evaluating thermal comfort at the air conditioning environment including the airport terminal [10,11], Thus only PMV index was calculated during the simulation. It considers many factors related to human thermal comfort and is calculated as follows [66]:

$$PMV = [0.303\exp(-0.036 M)+0.0275] \times \{M-W-3.05[5.733-0.007(M-W)-P_a]-0.42(M-W-58.2)-0.0173 M(5.867-P_a)-0.0014 M(34-t_a)-3.96 \times 10^{-8}f_{cl}[(t_{cl}+273)^4-(t_r+273)^4]-f_{cl}h_c(t_{cl}-t_a)\}, \tag{13}$$

where M is the energy metabolic rate of the human body, which is determined by the amount of human activity (W/m^2), as the passenger was slightly active, we took a value of $65 W/m^2$; W is the mechanical work done by the human body (W/m^2), it is generally taken as 0; P_a is the partial pressure of the water vapor around the human body (kPa), there is a certain connection between it and the air temperature [69] and the calculation formula is shown in the Supporting Information; t_a is the air temperature around the human

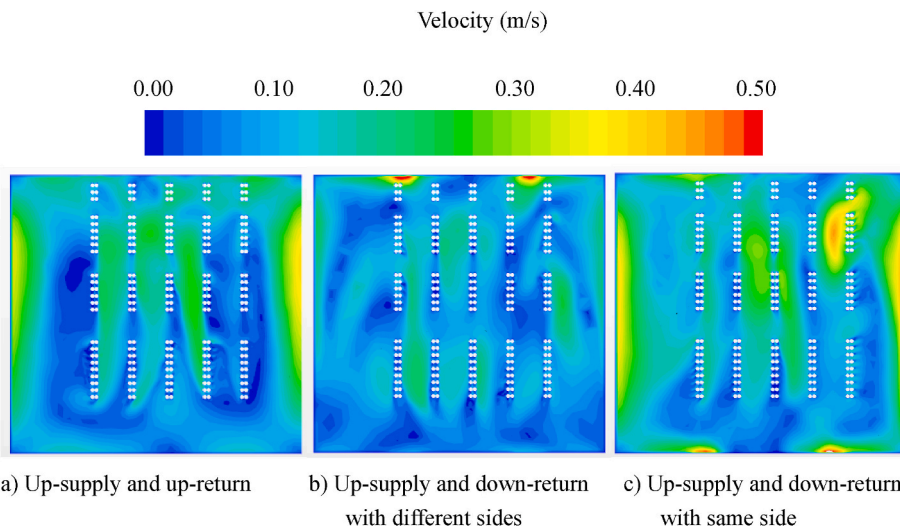


Fig. 9. The 1.2 m height plane wind velocity fields of three ventilation forms.

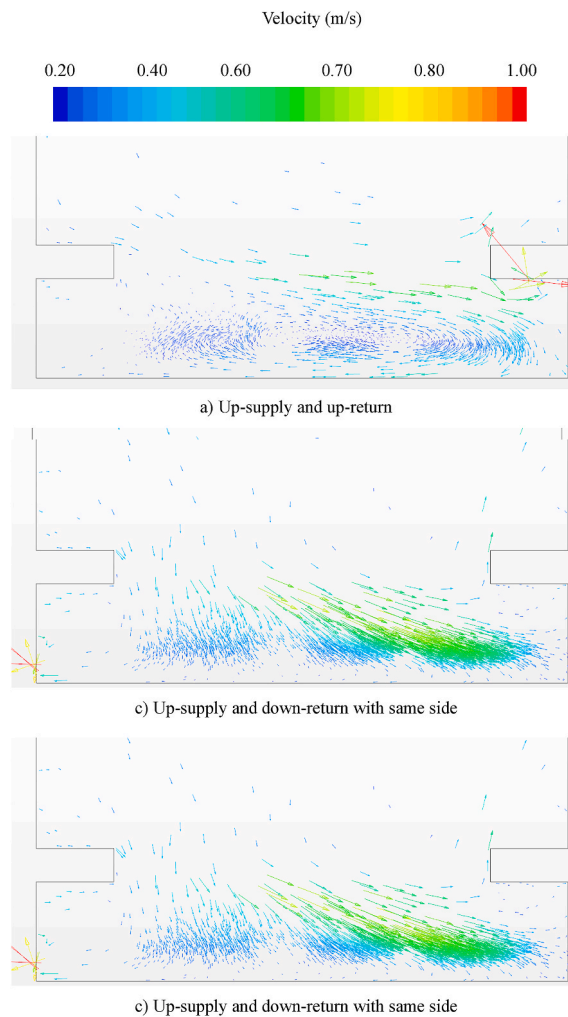


Fig. 10. Velocity streamline distribution in the vertical direction perpendicular to return air outlet.

Table 3

Average velocity of three ventilation forms(m/s).

	Up-supply and up-return	Up-supply and down-return with different sides	Up-supply and down-return with same side
Department hall	0.15	0.12	0.18
Respiratory region	0.13	0.1	0.16

body ($^{\circ}\text{C}$); t_r is the average radiation temperature; t_{cl} is the outer surface temperature of the clothes ($^{\circ}\text{C}$); h_c is the convective heat transfer coefficient [$\text{W}/(\text{m}^2\cdot\text{K})$], it was taken at $5.1 \text{ W}/(\text{m}^2\cdot\text{K})$ due to the indoor environment in the summer in our study; and f_{cl} is the clothing area coefficient. The calculation formula for the clothing area coefficient could also be found in the Supporting Information.

The PMV index represents the cold and hot feelings of the vast majority of people in the same environment and has a range of -3-3, wherein a value less than 0 means cold and a value greater than 0 means hot. This index can be used to evaluate whether a thermal environment is comfortable. The PMV field distribution characteristics of the breathing plane are shown in Fig. 11, and the PMV of the waiting area and the breathing area of people under the three types of ventilation are summarized in Table 4.

The PMV distribution characteristics of the breathing plane show that most areas are within $-0.5-0.5$, indicating that most people feel comfortable. Here high PMV values appearing around some passengers located at the bottom regions in Fig. 11 are attributed to the high temperature of air exhausted from the mouth or heated by human body. As you suggested, we added the vertical cross-section with streamlines in Fig. 10. The airflow patterns along the vertical direction indicated that a stagnant wake obviously appeared at the areas next to the side of the air supply outlet, just at the height of nearly 1.2 m that is consistent with the bottom regions in Fig. 11. Static airflow and the heating effect induced by human heat loss might contribute to a higher PMV values at the stagnant wake compared with higher airflow regions. In addition, as listed in Table 4, the PMV values in the department hall of the airport terminal

under the three ventilation forms are basically within 0.5, which meets the requirements of the air-conditioning design temperature. However, the PMV values in the respiratory region of the airport terminal under the three ventilation forms are exceeds 0.5, which may cause the level of thermal comfort to be “slightly warm” [70]. The increase in PMV near the breathing area of people may be because of the high occupancy concentration, which increases heat dissipation, causing the PMV to rise.

4.4. CO₂ concentration

4.4.1. CO₂ concentration analysis at the respiratory range

The CO₂ concentration distribution characteristics are shown in Fig. 12. In the airport department hall, the CO₂ concentration in most areas of the breathing plane is below 1000 ppm, which meets indoor air quality standards. However, because people exhale CO₂ continuously, the concentration of CO₂ in densely populated areas is relatively high, compared to other areas, some of which exceed 1000 ppm. In all three ventilation modes, the CO₂ concentrations near the side of the air supply were higher than that in other areas. This may be because of the higher position of the air supply outlet, which does not improve ventilation within the breathing area.

4.4.2. CO₂ concentration analysis along Z direction

To analyze the CO₂ concentration level in the vertical direction, we used different height planes to calculate the average CO₂ concentration, as shown in Fig. 13. First, the difference in the vertical CO₂ concentration distribution between up-supply and down-return with different sides and up-supply and down-return with the same side is very small, but it is significantly higher when the ventilation mode is up-supply and up-return. The maximum concentration difference is approximately 2 m in height, and the value for up-supply and up-return mode is approximately 27.39% higher than that for the up-supply and down-return with different sides. At approximately 1.5 m of the human breathing area, the value for the up-supply and up-return mode is approximately 23.7% higher than that for up-supply and down-return with different sides. Simultaneously, in a space below 2 m, it can be clearly seen that the CO₂ concentration of the up-supply and down-return with different sides mode was lower than that of the up-supply and down-return with the same side mode. Although this difference is slight, as passengers mainly live in a space below 2 m, we considered the up-supply and down-return with different sides mode to be better.

Fig. 13 shows that there is a significant increase in the CO₂ concentration near the breathing plane of the person. This indicates that breathing during high numbers of occupied passenger impacts the CO₂ concentration in the airport terminal. On this basis, it can be inferred that the CO₂ concentration in the terminal building is higher than usual when the airport has high numbers of occupied passenger.

4.4.3. CO₂ concentration analysis in the entire department hall

The average CO₂ concentrations in the department hall and the respiratory region are shown in Table 5. The CO₂ concentrations of the department hall and the respiratory region are both below 1000 ppm, and thus, meet air quality standards. However, regardless of ventilation form, the CO₂ concentration in the respiratory region is much higher than that of the department hall, proving that the breathing of people has a notable effect on the CO₂ concentration level in the airport terminal when there is high numbers of occupied passenger.

Table 5 shows that the up-supply and down-return with different sides and up-supply and down-return with the same side modes have better CO₂ discharge efficiency. In the terminal building, the CO₂ concentrations of these modes are approximately 12.53% and 4.66% lower, respectively, than the up-supply and up-return mode. Additionally, for the respiratory region, the CO₂ concentrations of these modes were approximately 20.04% and 15.00% lower, respectively, compared with the up-supply and up-return mode.

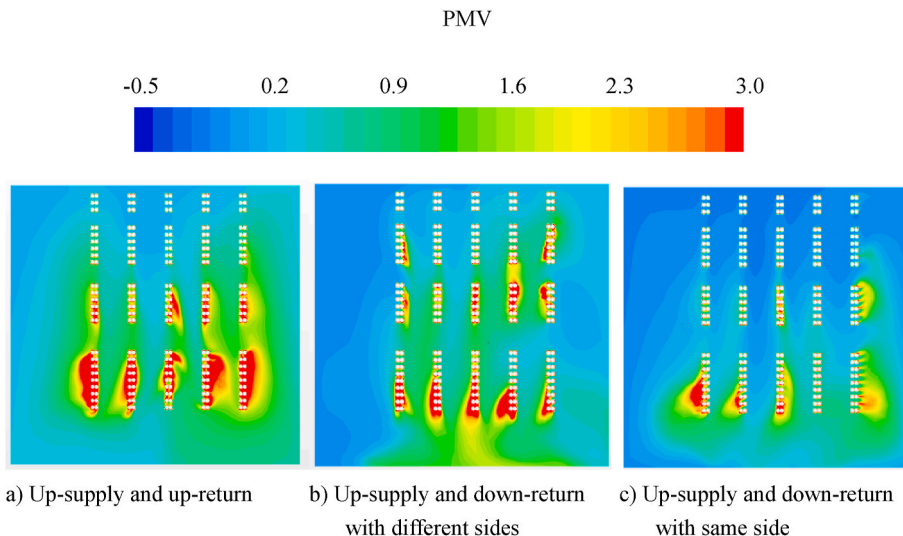


Fig. 11. The 1.2 m height plane predicted mean vote (PMV) fields of three ventilation forms.

Table 4
Predicted mean vote (PMV) values of three ventilation forms.

	Up-supply and up-return	Up-supply and down-return with different sides	Up-supply and down-return with same side
Department hall	0.28	0.22	0.07
Respiratory region	0.97	0.75	0.55

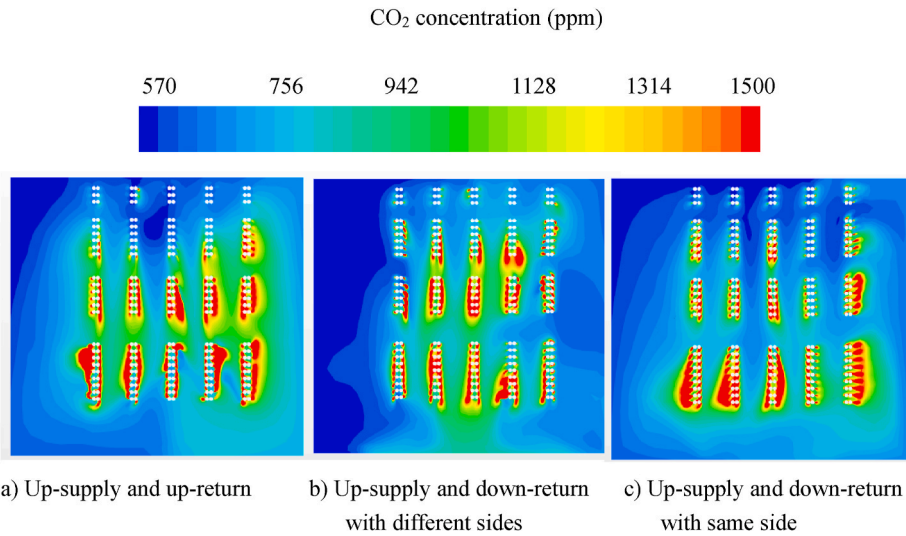


Fig. 12. The 1.2 m height plane CO₂ concentration fields for three ventilation forms.

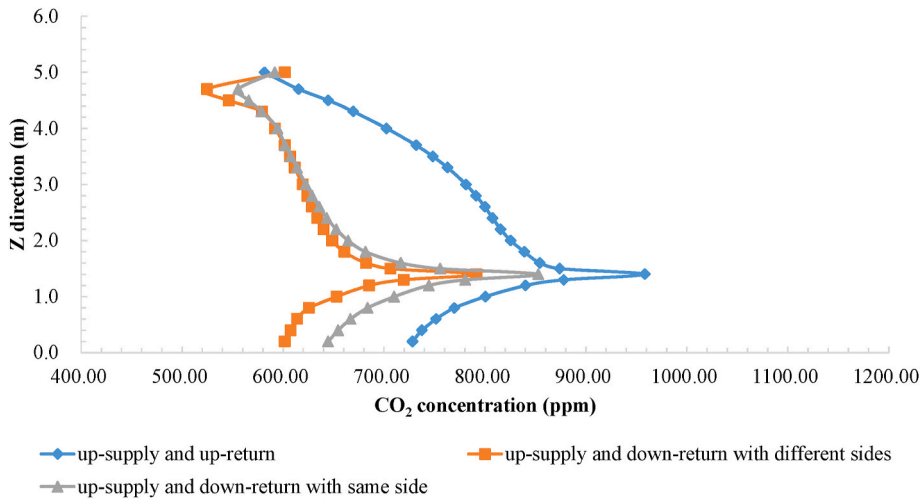


Fig. 13. CO₂ concentration levels in the vertical direction.

4.5. Aerosol diffusion

4.5.1. Characteristics of aerosol diffusion

In the aerosol diffusion simulation, we selected six representative locations to place infected persons, and assumed that they would

Table 5
CO₂ concentration values of three ventilation forms.

	Up-supply and up-return	Up-supply and down-return with different sides	Up-supply and down-return with same side
Department hall	605	529.19	576.78
Respiratory region	860.92	688.42	731.75

exhale harmful aerosol particles while breathing. The locations of the infected persons are marked with numbers in Fig. 14.

At present, many closed environments, such as aircraft cabins, carriages, classrooms, etc., have used the Wells-Riley model for exposure risk assessment [71–74], but this model is based on a quanta generation rate that is highly correlated with the type of virus. With regard to the emerging new coronavirus epidemic, we found that the “quanta” study of the novel coronavirus is still rare and there is no particularly clear figure. Therefore, we finally introduced the intake fraction (IF) for evaluation. The IF is a method to Inhalable factor is a method to evaluate the hazards of pollutants from the perspective of human health, which has been applied to the assessment of exposure levels in much environmental pollution. It refers to the ratio of the amount of a certain pollutant discharged by a certain emission source that is absorbed by the human body to the total emission [75,76], i.e., the exposure efficiency of the emission. And it can be defined as follows:

$$IF = \frac{\int_{t_1}^{t_2} C_{(t)} IR_{(t)} dt}{M_t(t_2 - t_1)} \quad (14)$$

where $C_{(t)}$ is the transient particle concentration simulated in the model (particles/m³); $IR_{(t)}$ is the human respiration rate (m³/s), for which the adult male and female average value is 1.835×10^{-4} m³/s; and M_t is the total amount of particles released by the particle emission source in a unit time period (particles/s), which was calculated to be 3291.5 particles/s for the human mouth area, respiration rate, and the exhaled volume of particles/unit area.

As there is currently no standard for the inhalation factor of PM in the environment, this study used the average inhalation factor of 0.00015 for underground garages, which was measured in a previous study [57], as the standard for dividing the probability of infection. Fig. 15 shows the iso-values of the particle concentration of the infected person at different positions during up-supply and up-return. Overall, areas with an IF exceeding 0.00015 form near the infected person (red in Fig. 15). This shows that breathing of the infected person will cause a different risk of infection at each location in the waiting hall. Regardless, the closer a passenger is to an infected person, the greater the risk of infection. Meanwhile, when consider the IF distribution along vertical direction, significant thermal plume around human body of infected person 3–6 that is far away from the air supply outlet climbed to almost 2.5 m high. Whereas, when infected person located near the air supply outlet that is Case 1 and 2 in the study, the thermal plume around the human body was destroyed due to the crosswind from the airflow inlet of ventilation systems. In addition, the closer the location is to the air supply side, the larger the area where the IF exceeds 0.00015. This suggests that the strong airflow on the air supply side causes PM to spread further.

4.5.2. Exposure level evaluation in the department hall

The volume-averaged IF values among three ventilation modes are listed in Table 6. When considering the averaged IF values in the whole department hall, up-supply and down-return with different sides could contribute to the lowest volume-averaged IF values among three ventilation modes, which is consistent with the results when considering CO₂ as index.

Whereas, as mentioned above, the differences in airflow patterns with the same ventilation rate might cause various aerosol transmission patterns. Thus, the volumes at which each infected person causes the IF to exceed 0.00015 under different ventilation modes are selected as another index when evaluating the aerosol transmission among three different ventilation modes and the results are listed in Table 7. Considering the high probability of infection, healthy people in an area where the IF exceeds 0.00015 will be infected. Therefore, the number of infected people near each patient is also listed in Table 7. The results show that the infected volumes caused by infected persons in the same position under different ventilation methods varied only slightly and were the largest at positions 1, 3, and 6. When the infected person is in position 1 or 6, the up-supply and down-return with the same side mode is more advantageous, whereas when the infected person is in position 3, the up-supply and down-return with different sides is more advantageous. By comparing the total volumes exceeding the IF in these six locations, we found that the up-supply and down-return with the same side had smaller volumes exceeding 0.00015, indicating that it had better ventilation.

It could be concluded that the optimized ventilation mode is different when considering volume-averaged CO₂ concentration and areas where the intake fraction (IF) exceeds 0.00015 and number of infected people as index, separately. Usually, up-supply and down-return with the different sides is verified as an effective ventilation mode with reasonable airflow patterns and high pollutant removal efficiency when considering the volume-averaged pollutant concentration as index in enclosed environment [77,78]. Whereas, when considering the range of aerosol transmission and the number of infected persons as index, to our knowledge, the up-supply and down-return with the same side in the study contributed to a better performance due to the restricted diffusion of aerosols and accumulation mainly at the respiratory region induced by the significant downward airflow at the lower areas in the vertical direction, shown in Fig. 10 c).

5. Study limitations

There are some limitations to this study that should be addressed in future work. First, because the airport terminal occupies a large area, and considering the accuracy and time of the calculation software, we examined only approximately one-third of the airport terminal area in the CFD calculation. Second, as the airport is a large transport hub, we only considered the scenario in which there was high numbers of occupied passenger, i.e., the situation where all the seats are full. However, in real life, airports do not always have high numbers of occupied passenger, meaning our data do not accurately reflect actual airport terminal data. In future studies, we will conduct research for different passenger flows. Third, we only evaluated three different ventilation modes, and thus, did not include all the ventilation modes employed at the airport. Further research is required to evaluate the efficacy of other ventilation modes.

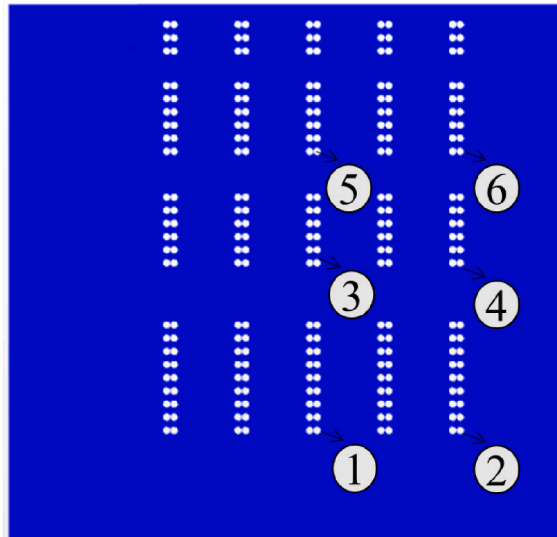


Fig. 14. Locations of infected persons in aerosol simulation.

6. Conclusions

In this research, the distribution characteristics of temperature, wind speed, PMV, and CO₂ and PM concentrations inside an airport terminal building were simulated using CFD simulation technology. According to a temperature analysis, the temperature in the department hall under the three ventilation modes should be maintained at 25–27 °C. However, the temperature in the respiratory region was higher, and the temperature of the department hall under the up-supply and up-return mode reached as high as 29.7 °C, indicating that its ventilation effect is poor. According to the wind speed analysis, the airflow distribution in the breathing plane of the up-supply and down-return with different sides ventilation mode was the most uniform, and there are fewer areas where the wind speed is greater than 0.3 m/s, compared with the other modes. Regarding the PMV of the respiratory plane, we found that the up-supply and down-return with the same side mode performed the best, followed by the up-supply and down-return with different sides and up-supply and up-return modes. For the three ventilation modes, the PMV values in the terminal building and the passenger breathing zone were in the range 0.07–0.28 and 0.55–0.97, respectively. The breathing zone PMV is much higher, indicating that the airport environment becomes hotter under high numbers of occupied passenger.

As an important simulation object in this study, we analyzed the CO₂ concentration field at the respiratory surface, the CO₂ concentration of the airport terminal, the CO₂ concentration in the respiratory area, and the vertical concentration distribution characteristics of the airport terminal. The results showed that the CO₂ concentration in the terminal building ranged between 500 ppm and 600 ppm. However, the concentration of CO₂ in the passenger breathing area was 26.8–42.3% higher than the CO₂ concentration in the terminal building under different ventilation modes. Considering the characteristics of the breathing zone and the overall and vertical distributions of CO₂ in the terminal building, we believe that the most suitable ventilation mode is up-supply and down-return with different sides.

By analyzing the diffusion characteristics of aerosol particles originating from infected persons in different locations under the three types of ventilation, we found that the up-supply and down-return with the same side mode was the best ventilation mode, which is inconsistent with the CO₂ diffusion results obtained. In addition, we found that the spread of particles in the middle position was larger, leading to a greater risk of inhalation for people around the infected person. Moreover, locations that were either close to the exit or were sparsely occupied had a lower risk of inhalation and a lower risk of infection.

CRedit authorship contribution statement

Yu Zhao: Conceptualization, Methodology, Writing – review & editing. **Yao Feng:** Model development, simulation and post-processing, Writing – original draft. **Liangdong Ma:** Visualization, Investigation, Supervision.

Declaration of competing interest

The authors declare that they have no known competing financial interests or personal relationships that could have appeared to influence the work reported in this paper.

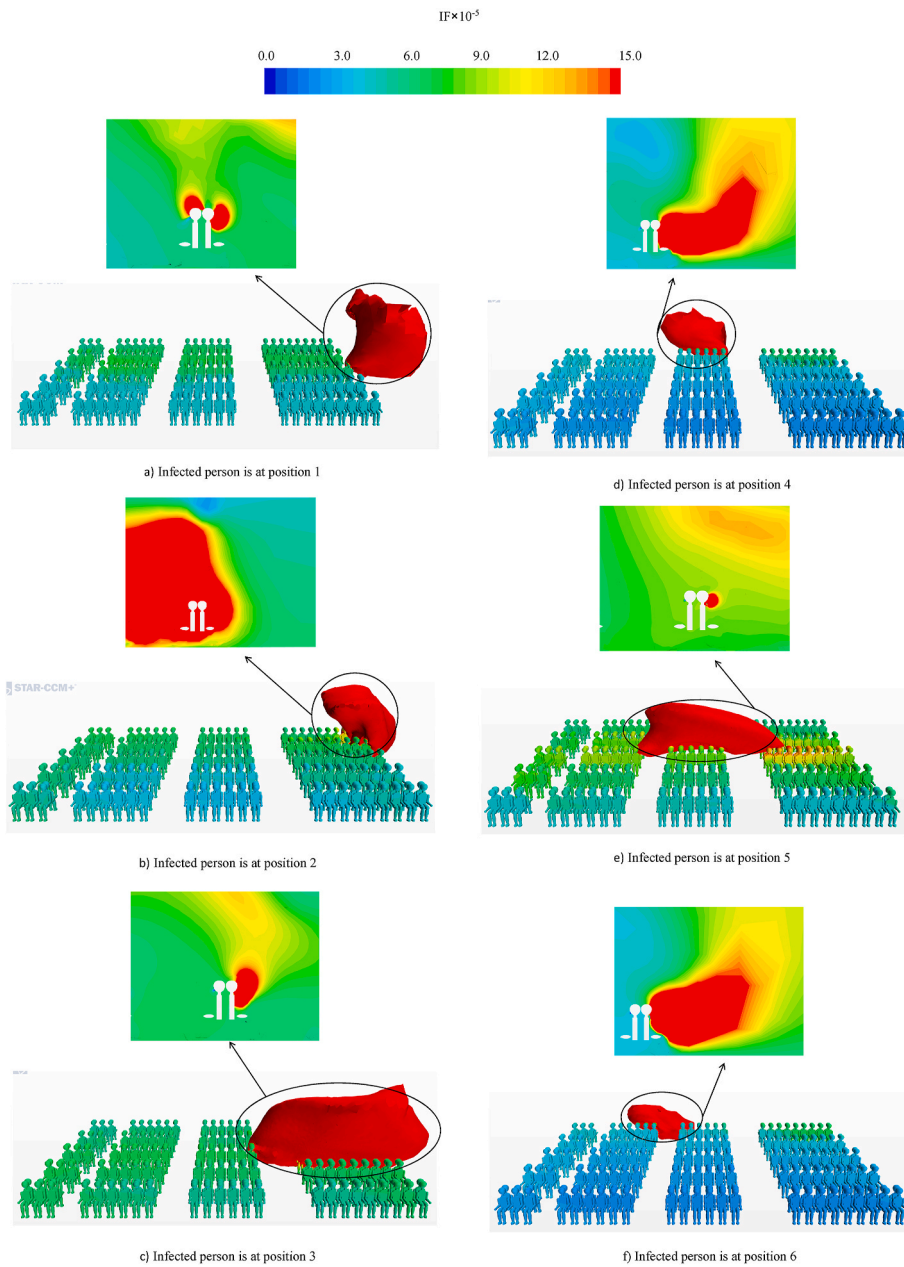


Fig. 15. Iso-value of the particle concentration 0.00015 during up-supply and up-return with the same side.

Table 6

IF values of three ventilation modes in the department hall (10⁻⁵).

Location of infected persons	Up-supply and up-return	Up-supply and down-return with different sides	Up-supply and down-return with same side
1	5.641	5.451	5.415
2	4.657	4.730	4.756
3	5.698	5.683	5.632
4	4.220	4.269	4.445
5	5.715	5.457	5.571
6	3.984	3.956	4.121
Average	4.986	4.925	4.990

Table 7

Areas where the intake fraction (IF) exceeds 0.00015 and number of infected people.

	Up-supply and up-return		Up-supply and down-return with different sides		Up-supply and down-return with same side	
	areas where IF exceeds 0.00015 (m ³)	infected people	areas where IF exceeds 0.00015 (m ³)	infected people	areas where IF exceeds 0.00015 (m ³)	infected people
1	67.99303	1	70.21412	1	45.95451	1
2	56.32360	3	53.35143	3	55.70668	3
3	96.35796	18	80.83378	18	95.52711	18
4	21.82193	2	22.96157	3	20.35877	1
5	38.67040	6	38.84560	7	40.27553	9
6	16.48970	1	16.16346	1	13.40250	0
Total	297.6566	31	282.37	33	271.2251	32

Acknowledgments

This work was sponsored by Department of Science and Technology of Liaoning Province (grant number: 2021JH2/10300002). We also would like to thank Editage (www.editage.cn) for English language editing.

Appendix A. Supplementary data

Supplementary data to this article can be found online at <https://doi.org/10.1016/j.job.2022.104276>.

References

- [1] J.Y. Chao, Design and operation status of ventilation and air conditioning terminal systems in airport terminals, *Heat. Vent. Air Cond.* 51 (2021) 67–72, 04.
- [2] Civil Aviation Resource Net of Chin, "The 14th Five-Year Plan" civil aviation infrastructure "construction drawings" emerge. <http://news.carnoc.com/list/556/556879.html>, 2021. (Accessed 16 March 2021).
- [3] Z.W. Wang, M.M. Zhao, H.X. Li, Study on operational performance forecast of 10 Asian hub airports, *Adv. Aeronaut. Sci. Eng.* 12 (4) (2021) 90–98, <https://doi.org/10.16615/j.cnki.1674-8190.2021.04.10>.
- [4] People's Daily Online, The international airport has become an important place for the spread of the epidemic, How should we deal with it?. <http://sn.people.com.cn/n2/2021/0802/c378287-34848419.html>, 2021. (Accessed 2 August 2021).
- [5] M.L. Pöhlker, O.O. Krüger, J.D. Förster, T. Berkemeier, W. Elbert, E. Mikhailov, Respiratory Aerosols and Droplets in the Transmission of Infectious Diseases, *arXiv preprint arXiv:2103.2021.01188*.
- [6] S. Asadi, A.S. Wexler, C.D. Cappa, S.B. Barreda, N.M. Bouvier, W.D. Ristenpart, Aerosol emission and super emission during human speech increase with voice loudness, *Sci. Rep-UK.* 9 (1) (2019) 1–10, <https://doi.org/10.1038/s41598-019-38808-z>.
- [7] M. Jayaweera, H. Perera, B. Gunawardana, J. Manatungea, Transmission of COVID-19 virus by droplets and aerosols: a critical review on the unresolved dichotomy, *Environ. Res.* 100 (2020) 476–482, <https://doi.org/10.1016/j.envres.2020.109819>.
- [8] Phoenix New, Nanjing Airport was lost and hundreds of people were infected in 5 provinces and 9 cities. Experts: the scale of the epidemic is still difficult to predict. <https://ishare.ifeng.com/c/s/88FbtoR6CIH>, 2021. (Accessed 28 July 2021).
- [9] Y. Yang, Ventilation system and comfort analysis of airport waiting hall, *Chin. Mark.* 19 (2011) 120–122.
- [10] J.Y. Zhang, M. Liu, L. Lin, H.H. Yang, Study on thermal comfort of impinging jet ventilation system applied to airport terminal buildings, *J. HV&AC* 45 (2015) 86–88+58, 03.
- [11] L. Li, H.H. Yang, C.D. Gan, Simulation of air-distribution of the stratified air-conditioning system for new aviation building of Hongqiao Airport, *Refrig. Air Cond.* 10 (2010) 77–80, 06.
- [12] X.Y. Jia, B. Cao, Y.X. Zhu, Y. Huang, Field studies on thermal comfort of passengers in airport terminals and high-speed railway stations in summer, *Build. Environ.* 206 (2021) 108319, <https://doi.org/10.1016/j.buildenv.2021.108319>.
- [13] X.Y. Jia, Y. Huang, B. Cao, Y.X. Zhu, C.W. Wang, Field investigation on thermal comfort of passengers in an airport terminal in the severe cold zone of China, *Build. Environ.* 189 (2021) 107514, <https://doi.org/10.1016/j.buildenv.2020.107514>.
- [14] A. Kotopoulos, M. Nikolopoulou, Evaluation of comfort conditions in airport terminal buildings, *Build. Environ.* 130 (2018) 162–178, <https://doi.org/10.1016/j.buildenv.2017.12.031>.
- [15] J.P. Duguid, The size and the duration of air-carriage of respiratory droplets and droplet-nuclei, *Epidemiol. Infect.* 44 (6) (1946) 471–479, <https://doi.org/10.1017/S0022172400019288>.
- [16] R.G. Loudon, R.M. Roberts, Relation between the airborne diameters of respiratory droplets and the diameter of the stains left after recovery, *Nature* 213 (5071) (1967) 95–96, <https://doi.org/10.1038/213095a0>.
- [17] P. Höpfe, Temperatures of expired air under varying climatic conditions, *Int. J. Biometeorol.* 25 (2) (1981) 127–132, <https://doi.org/10.1007/BF02184460>.
- [18] C.I. Fairchild, J.F. Stampfer, Particle concentration in exhaled breath, *Am. Ind. Hyg. Assoc. J.* 48 (11) (1987) 948–949, <https://doi.org/10.1080/15298668791385868>.
- [19] R.S. Papineni, F.S. Rosenthal, The size distribution of droplets in the exhaled breath of healthy human subjects, *J. Aerosol Med.* 10 (2) (1997) 105–116, <https://doi.org/10.1089/jam.1997.10.105>.
- [20] Morawska, Droplets expelled during human expiratory activities and their origins, in: *Proceeding of the 11th International Conference on Indoor Air Quality and Climate Change*, University of Denmark, Denmark, 2008, pp. 1–8.
- [21] H. Helene, L. Evert, A. Almstrand, B. Björn, A. Olin, Size distribution of exhaled particles in the range from 0.01 to 2.0µm, *J. Aerosol Sci.* 41 (2010) 439–446, <https://doi.org/10.1016/j.jaerosci.2010.02.011>.
- [22] Z. Wang, H.T. Zhao, B.R. Lin, Y.X. Zhu, Q. Ouyang, Y. Juan, Investigation of indoor environment quality of Chinese large-hub airport terminal buildings through longitudinal field measurement and subjective survey, *Build. Environ.* 94 (2015) 593–605, <https://doi.org/10.1016/j.buildenv.2015.10.014>.
- [23] National standards of the People's Republic of China, Design Code for Heating Ventilation and Air Conditioning of Civil Buildings GB50736-2012, China Architecture & Building Press, 2012.
- [24] Y. Geng, J. Yu, B.R. Lin, Z. Wang, Y.X. Huang, Impact of individual IEQ factors on passengers' overall satisfaction in Chinese airport terminals, *Build. Environ.* 112 (2017) 241–249, <https://doi.org/10.1016/j.buildenv.2016.11.040>.
- [25] J.J. Hong, B.R. Lin, The investigation of indoor air quality and ventilation of an airport terminal building in China, *IOP Conf. Ser. Mater. Sci. Eng.* 609 (3) (2019), 032051, <https://doi.org/10.1088/1757-899X/609/3/032051>.

- [26] X.C. Liu, L. Lin, X.H. Liu, T. Zhang, X.Y. Rong, L. Yang, D.Z. Xiong, Evaluation of air infiltration in a hub airport terminal: on-site measurement and numerical simulation, *Build. Environ.* 143 (2018) 163–177, <https://doi.org/10.1016/j.buildenv.2018.07.006>.
- [27] M.K. Akyüz, H. Kafali, O. Altuntas, Investigation of indoor air quality and thermal comfort condition in airport terminal buildings, *Aircraft Eng. Aero. Technol.* 93/1 (2021) 25–34, <https://doi.org/10.1108/AEAT-06-2020-0118>.
- [28] J.L. Ren, *Research on the Purification Effectiveness of Ventilation Filter Purification System on Indoor PM_{2.5} Particulate Pollutants*, Tianjin University, Tianjin, 2018.
- [29] Centers for Disease Control and Prevention (CDC), Indoor air quality at nine large-hub airports with and without designated smoking areas—United States, October–November 2012, *MMWR-Morbid. Mortal. Week. Rep.* 61 (46) (2012) 948–951, <https://doi.org/10.1108/AEAT-06-2020-0118>.
- [30] J.R. Ren, X.D. Cao, J.J. Liu, Impact of atmospheric particulate matter pollutants to IAQ of airport terminal buildings: a first field study at Tianjin Airport, China, *Atmos. Environ.* 179 (2018) 222–226, <https://doi.org/10.1016/j.atmosenv.2018.02.019>.
- [31] J.L. Ren, J.J. Liu, W.D. Li, Study on Fine Particle and Volatile Organic Pollutants in the Terminal Building of Tianjin Airport, China, *Proceedings of the 4th International Conference On Building Energy & Environment*, 2018, pp. 636–640.
- [32] A. Kim, L. Medal, S.Q. Wang, T. Larson, Indoor and outdoor concentrations of particulate matter in an airport Terminal building: a pilot study at Soekarno-Hatta international airport in Indonesia, *Buildings-Basel* 10 (2) (2020), <https://doi.org/10.3390/buildings10020025>.
- [33] S. Zanni, F. Lalli, E. Foschi, A. Bonoli, L. Mantecchini, Indoor air quality real-time monitoring in airport terminal areas: an opportunity for sustainable management of micro-climatic parameters, *Sensors* 18 (11) (2018), <https://doi.org/10.3390/s18113798>.
- [34] T.H. Shih, W.W. Liou, A. Shabbir, Z.G. Yang, J. Zhu, A new k-ε eddy viscosity model for high Reynolds number turbulent flows, *Comput. Fluid* 24 (3) (1995) 227–238, [https://doi.org/10.1016/0045-7930\(94\)00032-T](https://doi.org/10.1016/0045-7930(94)00032-T).
- [35] E. Rusly, L. Aye, W.W.S. Charters, A. Ooi, CFD analysis of ejector in a combined ejector cooling system, *Int. J. Refrig.* 28 (7) (2005) 1092–1101, <https://doi.org/10.1016/j.ijrefrig.2005.02.005>.
- [36] Z. Zhang, Q. Chen, Comparison of the Eulerian and Lagrangian methods for predicting particle transport in enclosed spaces, *Atmos. Environ.* 41 (25) (2007) 5236–5247, <https://doi.org/10.1016/j.atmosenv.2006.05.086>.
- [37] Y. Tominaga, T. Stathopoulos, Turbulent Schmidt numbers of CFD analysis with various types of flow field, *Atmos. Environ.* 41 (2007) 8091–8099, <https://doi.org/10.1016/j.atmosenv.2007.06.054>.
- [38] J. Han, Y. Li, R.Q. Jin, The influence of human walking on the flow and airborne transmission in a six-bed isolation room: tracer gas simulation, *Build. Environ.* 77 (2014) 119–134, <https://doi.org/10.1016/j.buildenv.2014.03.029>.
- [39] C. Chen, B. Zhao, Some questions on dispersion of human exhaled droplets in ventilation room: answers from numerical investigation, *Indoor Air* 20 (2) (2010) 95–111, <https://doi.org/10.1111/j.1600-0668.2009.00626.x> 95–111.
- [40] Z. Zhang, W. Zhang, Z.Q. Zhai, Q.Y. Chen, Evaluation of various turbulence models in predicting airflow and turbulence in enclosed environments by CFD: Part-2: comparison with experimental data from literature, *HVAC R Res.* 13 (6) (2007).
- [41] Z. Zhang, X. Chen, S. Mazumdar, T. Zhang, Q.Y. Chen, Experimental and numerical investigation of airflow and contaminant transport in an airliner cabin mockup, *Build. Environ.* 44 (1) (2009) 85–94, <https://doi.org/10.1016/j.buildenv.2008.01.012>.
- [42] Y. Zhao, S. Kato, J.N. Zhao, Characteristics of particle coagulation in an underground parking lot, *Environ. Sci. Pollut. Res.* 22 (2015) 18654–18668, <https://doi.org/10.1007/s11356-015-5590-4>.
- [43] Y. Zhao, P. Wang, L.D. Ma, J.L. Zhang, Prediction of pollutants dispersion patterns around two adjacent urban road tunnels, *J. Dispersion Sci. Technol.* 40 (2019) 82–93, <https://doi.org/10.1080/01932691.2018.1464469>.
- [44] Y. Zhao, J.N. Zhao, Numerical assessment of particle dispersion and exposure risk in an underground parking lot, *Energy Build.* 133 (2016) 96–103, <https://doi.org/10.1016/j.enbuild.2016.09.051>.
- [45] X. C. Song, Y. Zhao, Numerical investigation of airflow patterns and pollutant dispersions induced by a fleet of vehicles inside road tunnels using dynamic mesh part I: Traffic wind evaluation, *Atmos. Environ.*, 212 208–220. <https://doi.org/10.1016/j.atmosenv.2019.05.050>Get rights and content.
- [46] X.C. Song, Y. Zhao, Numerical investigation of airflow patterns and pollutant dispersions induced by a fleet of vehicles inside road tunnels using dynamic mesh part II: pollutant dispersion and exposure levels, *Atmos. Environ.* 210 (2019) 198–210, <https://doi.org/10.1016/j.atmosenv.2019.04.028>.
- [47] B. Zhao, C.Q. Yang, X.D. Yang, S.K. Liu, Particle dispersion and deposition in ventilated rooms: testing and evaluation of different Eulerian and Lagrangian models, *Build. Environ.* 43 (2008) 388–397.
- [48] A.C.K. Lai, Y.C. Cheng, Study of expiratory droplet dispersion and transport using a new Eulerian modeling approach, *Atmos. Environ.* 41 (2007) 7473–7484.
- [49] Z. Zhang, Q. Chen, Comparison of the Eulerian and Lagrangian methods for predicting particle transport in enclosed spaces, *Atmos. Environ.* 41 (25) (2007) 5236–5247, <https://doi.org/10.1016/j.atmosenv.2006.05.086>.
- [50] D. Gidaspow, C. Lin, Y.C. Seo, Fluidization in two-dimensional beds with a jet. 1. Experimental porosity distributions, *Ind. Eng. Chem. Res.* 22 (2) (1983) 187–193, <https://doi.org/10.1021/i100010a007>.
- [51] K. Haslbeck, K. Schwarz, J.M. Hohlfeld, J.R. Seume, W. Koch, Submicron droplet formation in the human lung, *J. Aerosol Sci.* 41 (2010) 429–438.
- [52] W.F. Wells, On air-borne infection: study II droplets and droplet nuclei, *Am. J. Epidemiol.* 20 (3) (1934) 611–618, <https://doi.org/10.1093/oxfordjournals.aje.a118097>.
- [53] L. Morawska, Droplet fate in indoor environments, or can we prevent the spread of infection? *Indoor Air* 16 (5) (2006) 335–347.
- [54] D. Rim, M. Green, L. Wallace, A. Persily, J. Choi, Evolution of ultrafine particle size distributions following indoor episodic releases: relative importance of coagulation, deposition and ventilation, *Aerosol Sci. Technol.* 46 (5) (2012) 494–503, <https://doi.org/10.1080/02786826.2011.639317>.
- [55] J. Corner, E.D. Pendlebury, The coagulation and deposition of a stirred aerosol, *Proc. Phys. Soc.* 64 (8) (1951) 645, <https://doi.org/10.1088/0370-1301/64/8/304>.
- [56] A. Lai, W.W. Nazaroff, Modeling indoor particle deposition from turbulent flow onto smooth surfaces, *J. Aerosol Sci.* 31 (4) (2000) 463–476, [https://doi.org/10.1016/S0021-8502\(99\)00536-4](https://doi.org/10.1016/S0021-8502(99)00536-4).
- [57] Y. Zhao, *Research on PM_{1.0} Dynamic and Dispersion Characteristics at Residential Underground Parking Lot in a Natural State*, Harbin Institute of Technology, Harbin, 2016.
- [58] C. Wu, R. Zhang, S. Liu, Air conditioning system Analysis of large airport terminal building, *Construct. Des. Eng.* 10 (2015) 88–90+95, <https://doi.org/10.13616/j.cnki.gcjsysj.2015.10.020>.
- [59] K. Zhao, X.H. Liu, Y. Jiang, On-site measured performance of a radiant floor cooling/heating system in Xi'an Xianyang International Airport, *Sol. Energy* 108 (2014) 274–286, <https://doi.org/10.1016/j.solener.2014.07.012>.
- [60] Z. Tao, X. Liu, Z. Lun, J. Jiang, Z. Min, J. Yi, Performance analysis of the air-conditioning system in Xi'an Xianyang international airport, *Energy Build.* 59 (2013) 11–12, <https://doi.org/10.1016/j.enbuild.2012.12.044>.
- [61] B. Zhuang, J. Shi, Z. Chen, Numerical study on indoor environment and thermal comfort in train station waiting hall with two different air-conditioning modes, *Build. Simul.* 14 (2021) 337–349, <https://doi.org/10.1007/s12273-020-0732-0>.
- [62] K. Zhao, J.T. Weng, J. Ge, On-site measured indoor thermal environment in large spaces of airports during winter, *Build. Environ.* 167 (2020) 106463, <https://doi.org/10.1016/j.buildenv.2019.106463>.
- [63] CD-adapco, *USER GUIDE STAR-CCM+ Version 8.02*, CD-adapco, New York, 2013.
- [64] R.Y. Zhao, C.Y. Fan, D.H. Xue, Y.M. Qian, *Air Conditioning*, fourth ed., China Architecture & Building Press China, 2009.
- [65] Z.S. Wang, T. Wu, X.L. Duan, S. Wang, W.J. Zhang, X. F. Wu, Y.J. Yu, Research on inhalation rate exposure factors of Chinese residents in environmental health risk assessment, *Res. Environ. Sci.* 22 (10) (2009) 1171–1175, <https://doi.org/10.13198/j.res.2009.10.61.wangzsh.007>.
- [66] Y.X. Zhu, *Built Environment*, fourth ed., China Architecture & Building Press, China, 2010.
- [67] X. Chen, Y. Lv, Y.W. Zhou, B. Chen, Y.N. Tian, X. Liu, Y.C. Yang, Study on permeability coefficient and bacterial composition, diversity and sources of indoor and outdoor fine particles of ten cities in northeast China, *Environ. Chem.* 39 (5) (2020) 1169–1180.

- [68] Y.S. Huang, W.X. Deng, J.W. Liao, X.H. Chen, X.Q. Zhou, Simulation research on air distribution of air conditioning in main terminal building of Guangzhou Baiyun airport, *Fluid Mach.* 39 (11) (2011) 74–76.
- [69] D.D. Shen, Y.G. Tong, *Engineering Thermodynamics, fifth ed.*, Higher Education Press, China, 2016.
- [70] K.H. Kim, S.Y. Kang, J.H. Lee, M.D. Oh, Analysis of thermal environment in an airport passenger terminal, *Numer. Heat. Tr. A-Appl.* 40 (5) (2001) 531–541, <https://doi.org/10.1080/10407780152619829>.
- [71] Z. Cheng, A. Aganovic, G.Y. Cao, Z.M. Bu, Experimental and simulated evaluations of airborne contaminant exposure in a room with a modified localized laminar airflow system, *Environ. Sci. Pollut. Res.* 28 (2021) 30642–30663, <https://doi.org/10.1007/s11356-021-12685-4>.
- [72] D. Licina, Y.L. Tian, W.W. Nazaroff, Inhalation intake fraction of particulate matter from localized indoor emissions, *Build. Environ.* 123 (2017) 14–22, <https://doi.org/10.1016/j.buildenv.2017.06.037>.
- [73] G. Habelomatis, A. Chaloulakou, A CFD modeling study in an urban street canyon for ultrafine particles and population exposure: the intake fraction approach, *Sci. Total Environ.* 530–531 (2015) 227–232, <https://doi.org/10.1016/j.scitotenv.2015.03.089>.
- [74] J.S. Russo, H.E. Khalifa, CFD assessment of intake fraction in the indoor environment, *Build. Environ.* 45 (2010) 1968–1975, <https://doi.org/10.1016/j.buildenv.2010.01.017>.
- [75] W.W. Nazaroff, Inhalation intake fraction of pollutants from episodic indoor emissions, *Build. Environ.* 43 (3) (2008) 269–277, <https://doi.org/10.1016/j.buildenv.2006.03.021>.
- [76] P. Kumar, M. Ketzler, S. Vardoulakis, L. Pirjola, R. Britter, Dynamics and dispersion modelling of nanoparticles from road traffic in the urban atmospheric environment-A review, *J. Aerosol Sci.* 42 (9) (2011) 580–603, <https://doi.org/10.1016/j.jaerosci.2011.06.001>.
- [77] Z. Zhang, *Study on the Influences of Air Flow Pattern on Contaminant Distribution in Laboratory*, Guangzhou University, Guangzhou, 2015.
- [78] X. Lv, X. Liu, M. Wu, Z. Peng, Comparison of airflow and pollutant dispersion in multi-room buildings under different cross-ventilation patterns, in: *Proceedings of the 11th International Symposium on Heating, Ventilation and Air Conditioning, ISHVAC, 2019*, pp. 1383–1391.